ARTICLE

Modeling Study of Hydrogen/Oxygen and n-alkane/Oxygen Counterflow Diffusion Flames

Xiao-wei Wang[a], Guo-biao Cai[a*], Vigor Yang[b]

a. School of Astronautics, Beijing University of Aeronautics and Astronautics, Beijing 100191, China
b. School of Aerospace Engineering, Georgia Institute of Technology, Atlanta GA, 30332 USA

A comprehensive analysis of hydrogen/oxygen and hydrocarbon/oxygen counterflow diffusion flames has been conducted using corresponding detailed reaction mechanisms. The hydrocarbon fuels contain n-alkanes from CH_4 to $C_{16}H_{34}$. The basic diffusion flame structures are demonstrated, analyzed, and compared. The effects of pressure, and strain rate on the flame behavior and energy-release rate for each fuel are examined systematically. The detailed chemical kinetic reaction mechanisms from Lawrence Livermore National Laboratory (LLNL) are employed, and the largest one of them contains 2115 species and 8157 reversible reactions. The results indicate for all of the fuels the flame thickness and heat release rate correlate well with the square root of the pressure multiplied by the strain rate. Under the condition of any strain rate and pressure, H_2 has thicker flame than hydrocarbons, while the hydrocarbons have the similar temperature and main products distributions and almost have the same flame thickness and heat release rate. The result indicates that the fuels composed with these hydrocarbons will still have the same flame properties as any pure n-alkane fuel.

Key words: Counterflow, Combustion, Hydrogen, Hydrocarbon, Flame

I. INTRODUCTION

Laminar counterflow diffusion flames provide much useful information about the basic properties of non-premixed combustion. A thorough understanding of strained laminar flames is a prerequisite to achieve improved knowledge of more complex system. As the important practical fuels in various propulsion and energy-conversion applications such as internal combustion engines, gas turbine combustors and rocket engines, combustions of hydrogen and hydrocarbon fuels are very valuable to investigate. For the studies on the flame properties of hydrocarbons, they always focus on the counterflow diffusion flames of n-alkane (C_nH_{2n+2}). To date, most existing studies of counterflow diffusion flames have been carried out on simple fuels such as hydrogen and methane, while the studies on high hydrocarbon fuels are less well documented. The main reasons are lack of the detailed reaction mechanisms validated in large ranges of conditions and the computational intensity with large detailed reaction mechanism is severe, especially for high hydrocarbons. High hydrocarbon fuels are extensively used in practical devices, while the investigations of their counterflow diffusion flames are less reported. Additionally, almost the current studies always only focus on one pure fuel. The

difference and relation of combustion flames of these fuels are still not clear. Ribert *et al.* established a framework to study on counterflow diffusion flames for hydrogen/oxygen mixture over the entire regime of thermodynamic states, and the effects of the pressure and strain rate were investigated [1]. The H_2/O_2 reaction mechanism in Ref.[2] involved 8 species and 19 reversible reactions. Pons *et al.* studied the mass transfer mechanism in transcritical methane diffusion counterflows with a reduced reaction mechanism containing 29 species and 141 reactions [3]. Tosatto *et al.* analyzed the chemical structure of a methane counterflow diffusion flame doped with small amounts of either JP-8 or a jet fuel surrogate using gas sampling via quartz microprobes and subsequent GC/MS analysis [4]. For high hydrocarbon, normal heptane (n-C_7H_{16}) is a representative higher hydrocarbon fuel, thus, the related studies always focused on n-heptane. Li and Williams carried out two experiments on n-heptane diffusion flame and partially premixed flame respectively [5]. The flame structures were calculated with a reduced mechanism involving 36 species and 180 elementary reactions. Difference between the experimental and calculation data indicated that the fuel chemistry required further attention. Seiser *et al.* performed a study to elucidate the mechanisms of extinction and autoignition of n-heptane counterflow diffusion flames [6]. Two reduced mechanism with 159 species and 770 reversible reactions, and 282 species and 1282 reversible reactions respectively, were developed from the previous detailed mechanism.

---

*Author to whom correspondence should be addressed. E-mail: cgb@buaa.edu.cn

231

Dakhlia *et al.* studied the Ludwig-Soret effects on *n*-Heptane/O_2/N_2 counterflow diffusion flames using a reduced mechanism involving 41 species and 273 elementary reactions [7]. The Ludwig-Soret effect was found negligible for this flame. Xue *et al.* used a reaction mechanism consisting of 41 species and 275 elementary reactions to investigate the structure and extinction of *n*-heptane/air partially premixed counterflow flames [8]. Zhu and Gore studied the flame structure and soot formation on hepante/air counterflow diffusion flame in certain experimental conditions [9]. Two different mechanisms were used. One consists of 41 species and 275 elementary reactions and the other of 180 species and 848 elementary reactions. Liu *et al.* investigated the effects of strain rate on high-pressure nonpremixed *n*-heptane autoignition in counterflow [10]. A reduced mechanism with 18 global reaction steps and a skeletal mechanism with 43 species and 185 reactions were used.

In 2006, Liu *et al.* successively numerically studied the effect of unsteady strain on *n*-heptane autoignition at elevated pressure in the counterflow configuration [11]. The skeletal reaction mechanism used in their previous study was still employed. Berta *et al.* conducted an experimental and numerical investigation of prevaporized *n*-heptane nitrogen-diluted nonpremixed flames [12]. A *n*-hepatne/air counterflow flame configuration is employed, and the major objective is to provide well-resolved experimental data regarding the structure and emission characteristics of these flames. The measurements are compared with predictions using a detailed *n*-heptane oxidation mechanism that includes the chemistry of NO_x and polycyclic aromatic hydrocarbon formation. Additionally, for other studies on *n*-heptane combustion, flame structure and extinction [13−15], and liquid-pool flames [16−18], *etc.* were investigated with reduced chemical mechanisms. For C_8−C_{16}, some studies on their reaction mechanisms have been carried out [19−28], while no study on counterflow diffusion flame with detailed mechanism was documented.

In the corresponding computational cost, the cost for the chemical rate evaluation scales linearly with the number of species, while the cost for the diffusion evaluation scales at least quadratically with the number of species [29]. Thus, complex mechanism brings the computational intensity and even is not able to obtain stable converged solutions, particularly under high pressure and strain. Therefore, in spite of many previous investigations, most of these studies, however, were carried out at low pressures, low strain rate or with reduced kinetic schemes. There is a paucity of study on the high hydrocarbon counterflow diffusion flame with detailed mechanism.

Concerning the study on reaction mechanism of hydrocarbon combustion, Simmie gave a comprehensive review of detailed mechanisms of hydrocarbon fuels [30]. Many efforts have been performed on the reaction mechanisms, but detailed mechanisms have been less developed, especially for high hydrocarbons. For the rep-

resentative fuel *n*-heptane, Ranzi *et al.* developed a semi-detailed kinetic scheme for *n*-heptane oxidation [31]. Lindstedt *et al.* developed a reaction mechanism involving 109 species and 659 reactions of *n*-heptane combustion [18]. A comprehensive detailed one involving 556 species and 2540 reversible reactions was developed by Curran and his coworkers from Lawrence Livermore National Laboratory (LLNL) [32]. This mechanism had been validated in wide ranges of combustion regimes and conditions, including high pressure region. To date, this scheme is still the most comprehensive one which has been validated in large ranges of conditions and combustion regimes. For other higher hydrocarbons, some studies on their reaction mechanisms had been carried out in France, Germany, Russia, US, *etc.* [19−28]. In 2009, LLNL developed a comprehensive detailed reaction mechanism for combustion of C_8−C_{16} *n*-alkanes hydrocarbons [24]. These mechanisms had also been validated in a wide variety of different sources and were recommended by other researchers [33, 34]. In addition, LLNL also developed and updated a series of comprehensive detailed reaction mechanisms for combustion of H_2 and C_1−C_4 *n*-alkanes hydrocarbons [35, 36]. In this work, those mechanisms from LLNL will be employed to model H_2 and C_1−C_{16} *n*-alkanes hydrocarbons combustion in counterflow configurations.

In order to reveal non-premixed combustion flame behaviors of H_2 and normal-alkanes (C_1−C_{16}) and to obtain the distinctions and relationship among them, a comprehensive investigation on the H_2 and hydrocarbon counterflow diffusion flame behaviors in large ranges of conditions was carried out. The effect of pressure and strain rate on the flame structure and heat release rate will be examined systematically for each fuel and compared with others. The comprehensive detailed mechanisms are employed. The results will also serve as a fundamental tool for establishing flame submodels for treating turbulent combustion (*e.g.* Flamelet turbulence combustion model [37]) over a wide range of conditions and a primary study on the commercial fuels combustion flame behaviors.

II. REACTION MECHANISM AND COMPUTATIONAL METHOD

To have a most appropriate investigation and comparison, the detailed reaction mechanisms developed by one organization (LLNL) [24, 32, 35, 36] are mainly employed in the present study. The mechanism of H_2 and CH_4−C_4H_{10} are updated by 2004. Those of C_7H_{16}−$C_{16}H_{34}$ were developed or updated in Dec 2009. The largest mechanism contains 2115 species and 8157 reversible reactions for $C_{16}H_{34}$ [38]. Those mechanisms had been validated in wide ranges of combustion regimes and conditions, including high pressure region. The specific reaction mechanism for each fuel is introduced in Table I.

The modeling computations were performed using

TABLE I Introduction of the reaction mechanisms for H_2, C_1-C_{16} counterflow diffusion flames modeling [38].

| Fuel	Status	Number of species	Number of reactions	References
H_2	Developed in 2004	9	21 reversible	[35]
CH_4	Developed in 1998/updated in 2004	155	689	[36]
C_2H_6	Developed in 1998/updated in 2004	155	689	[36]
C_6H_8	Developed in 1998/updated in 2004	155	689	[36]
C_4H_{10}	Developed in 1998/updated in 2004	155	689	[36]
C_5H_{12}	Developed in 1998/updated in Dec 2009	560	2539 reversible	[32]
C_6H_{14}	Developed in 1998/updated in Dec 2009	560	2539 reversible	[32]
C_7H_{16}	Developed in 1998/updated in Dec 2009	560	2539 reversible	[32]
C_8H_{18}	Developed in 2009/updated in Dec 2009	691	2992 reversible	[24]
$C_{10}H_{22}$	Developed in 2009/updated in Dec 2009	952	3899 reversible	[24]
$C_{12}H_{26}$	Developed in 2009/updated in Dec 2009	1078	5056 reversible	[24]
$C_{14}H_{30}$	Developed in 2009/updated in Dec 2009	1666	6476 reversible	[24]
$C_{16}H_{34}$	Developed in 2009/updated in Dec 2009	2115	8157 reversible	[24]
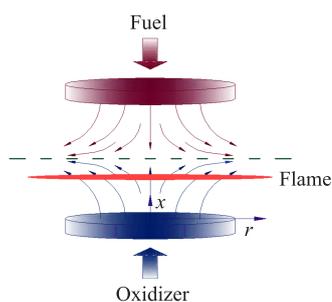
FIG. 1 Schematic of a counterflow diffusion flame.

the CHEMKIN PRO [39] suite of software in conjunction with the OPPDIF program [40]. The governing equations for the counterflow diffusion flame regime have been well documented and will not be discussed in detailed here; the reader is referred to the relevant reports for further information. The OPPDIF code computes the structure of the flame stabilized in the vicinity of the stagnation plane formed between two impinging, laminar, axisymmetric, and opposed streams. Figure 1 shows a schematic illustration of a counterflow configuration. Two infinitely wide circular nozzles directed toward each other at a fixed distance. One stream contains fuel and the other oxidizer. OPPDIF solves the temperature, species, mole fractions, axial and radial velocity components, the pressure gradient, and *etc.* for the diffusion flame.

The momenta of the counterflowing reactant streams $\rho_f V_f^2$ and $\rho_o V_o^2$ at the boundaries are kept almost equal to each other. Here, ρ_f and ρ_o represent the density of fuel and oxidizer, respectively. This condition ensures that the stagnation plane formed by the two streams is approximately in the middle of the region. The strain rate is defined as the normal gradient of the normal component of the flow velocity. The characteristic strain rate on the oxidizer side of the stagnation

TABLE II The critical points of n-alkane fuels.

Chemical formula (name)	$p_c{}^{\text{a}}$/MPa	$T_c{}^{\text{b}}$/K
CH_4 (methane)	4.58	190.7
C_2H_6 (ethane)	4.82	305.5
C_6H_8 (propane)	4.21	370.0
C_4H_{10} (butane)	3.75	425.2
C_5H_{12} (pentane)	3.36	469.8
C_6H_{14} (hexane)	3.01	507.4
C_7H_{16} (heptane)	2.74	540.3
C_8H_{18} (octane)	2.49	568.9
$C_{10}H_{22}$ (decane)	2.10	617.0
$C_{12}H_{26}$ (dodecane)	1.82	658.2
$C_{14}H_{30}$ (tetradecane)	1.44	693
$C_{16}H_{34}$ (hexadecane)	1.41	722

a p_c is critical pressure.
b T_c is critical temperature.

plane, a, is presumed to be give by [41].

$$a = \frac{2\,|V_o|}{L}\left(1 + \frac{|V_f|\,\sqrt{\rho_f}}{|V_o|\,\sqrt{\rho_o}}\right) \tag{1}$$

L is the distance between fuel and oxidizer inlets, V and ρ are the normal flow velocities and density. Subscripts f and o are the fuel and oxidizer. The distances between the fuel and oxidizer port are set at 2.0 cm.

III. RESULTS AND DISCUSSION

The critical points of these fuels are shown in Table II. The critical temperature of $C_{16}H_{34}$ is above 700 K, because the calculation pressure will be below the critical pressure, and in order to mainly investigate the fundamental flame behaviors, the fuels are all set at prevaporized states in this study, thus inlet temperatures

are typically set at 800 K in this work. The pressure ranges form 0.1 MPa to 1.0 MPa, and the strain rate is practically chosen from 10 s^{-1} to 10^6 s^{-1}.

A. H$_2$, hydrocarbons/O$_2$ counterflow diffusion flames

Figure 2 shows the flame temperature and main species mole fraction distributions at a typical condition (*i.e.*, p=1.01 MPa, a=1000 s^{-1}) of each fuel. All of the species with value of maximum mole fraction more than 0.1 are demonstrated. Here, fuel inlets are at left side, and oxygen inlets are at the right side. All of the flames have established themselves on the oxygen sides, with the nearer distance from the stagnation planes for the higher hydrocarbon. The temperatures reach maximum values of 3440, 3332, 3380, and 3375 K for C$_0$, C$_1$, C$_7$, and C$_{16}$ at 1.01 MPa (H$_2$, here, is considered as C$_0$H$_2$). The flame thickness δ_f, defined as the full width at half maximum value of temperature, is 0.83, 0.59, 0.6, and 0.62 mm for these cases. It can be seen that the H$_2$ flame thickness is obviously bigger than others, while the flame temperature profiles of C$_1$−C$_{16}$ are very similar and the corresponding flame thickness is almost the same. For all the fuels, the locations of maximum flame temperatures are almost the same as those of maximum H$_2$O mole factions. The major products of combustion of H$_2$ are H$_2$O and OH, beside these two species, CO, CO$_2$, and H$_2$ become the major products for hydrocarbons. Additionally, the hydrocarbon higher than C$_5$, C$_2$H$_2$ and C$_2$H$_4$, also reach notable concentrations. These results show that the mole fractions of carbon-containing products increase for higher hydrocarbons. The primary product is still H$_2$O for C$_1$ due to the low fraction of carbon in methane, while CO becomes the primary product from C$_2$ and then increases successively from C$_2$−C$_{16}$, and the fraction of H$_2$O decreases correspondingly. As an example, it can be seen that the primary product of C$_7$ combustion is CO, followed by H$_2$O, H$_2$, CO$_2$, OH, C$_2$H$_4$, and C$_2$H$_2$. The major hydrocarbon products are all consumed before the stoichiometric mixture fraction (the mixture faction at stoichiometric state, 1.724 mm for C$_7$, the corresponding location is 9.517 mm). Hydrogen can be observed to break through the stoichoimetric position and pass the point of maximum temperature for hydrocarbon combustion, and the radical OH peaks on the lean side.

Absolutely, there are some differences among these flame structures, while the main species distributions of all the fuels are similar except H$_2$. Figure 3 shows the maximum flame temperature, flame thickness and heat release rate per unit area as a function of carbon number in these fuels. The heat release rate per unit area $\dot{q}_s$ is defined as:

$$\dot{q}_s = \int_{-\infty}^{+\infty} \left(\sum_{k=1}^{N_S} \bar{h}_k W_k \dot{w}_k \right) \mathrm{d}y \qquad (2)$$

Compared with hydrocarbon combustion, H$_2$/O$_2$

flame has the much thicker flame thickness and higher flame maximum temperature, which can be interpreted by the less diffusivity of the hydrocarbons than hydrogen and higher enthalpy of H$_2$. For the hydrocarbon fuels, the higher hydrocarbon has little higher maximum temperature and thicker flame thickness, less heat release rate. However, the effect of the number of carbon is very limited and these results seem almost the same, which can be understood from the main species distributions for hydrocarbon fuels shown in Fig.2. The limited difference among the species distributions causes the limited different results shown in Fig.3. It can also be seen that the maximum flame temperature and heat release rate profiles have little valleys at C$_1$, because of the particular product distributions caused by its low ratio of C to H.

B. Effect of pressure and strain rate

In order to further investigate the flame properties of these fuels, a large range of pressure and strain rate was calculated. To have a fair comparison, the ranges of pressure and strain rate were set the same for all the fuels. Pressure ranges from 0.1 MPa to 10.1 MPa and strain rate from 10 s^{-1} to 10^6 s^{-1}. As an example, Fig.4 shows the temperature distributions for the C$_1$ cases at different pressures at a typical strain rate (*i.e.*, a=1000 s^{-1}). The temperatures reach maximum values of 2584, 3332, 3578, and 3686 K for the C$_1$ cases at 0.1, 1.01, 5.05, and 10.1 MPa, respectively. δ_f are 1.84, 0.59, 0.26, and 0.18 mm at 0.1, 1.01, 5.05, and 10.1 MPa, respectively. The influence trend of pressure on the counterflow diffusion flame structure also can be found. A pressure increase in a combustion system reduces the amount of dissociation of the compounds in products, and the maximum flame temperature increases. However, δ_f exhibits an opposite trend. The systematic calculations at difference pressures also had been conducted for other fuels. Figure 5 shows the reduction of the flame thickness with pressure for all the fuels at the typical strain rate of 1000 s^{-1}. As a given strain rate, the pressure always shows a linear dependence of the flame thickness for each fuel. At all the pressure range, the H$_2$ flames always are thicker than all of the hydrocarbons. All of the hydrocarbons have almost the same flame thickness at any pressure. Additionally, the same linear relationships between pressure and flame thickness have been revealed due to all the results collapse into a single line for the *n*-alkanes. These phenomena can be further explored by considering the heat release rate per unit flame area shown in Fig.6.

Figure 6 shows that the heat release rate increases with pressure. At a given strain rate, the pressure always shows a linear dependence of the heat release rate for each fuel. Similar to the flame thickness behavior, the heat release rate of all the *n*-alkane fuels are almost the same at any pressure.

Figure 7 shows the maximum flame temperature $T_{\max}$
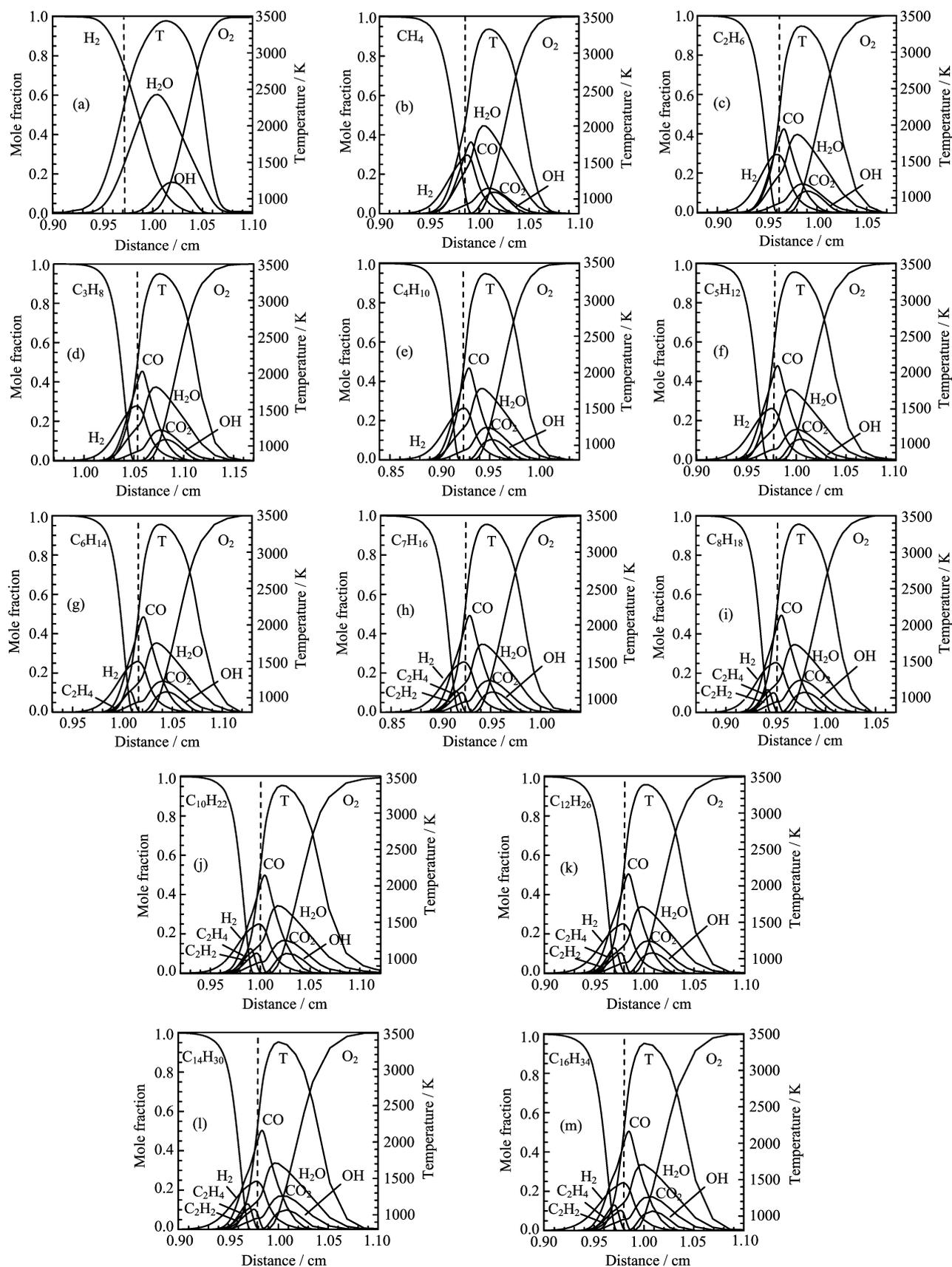
FIG. 2 The flame temperature and main species profiles for H_2, C_1-C_{16} n-alkanes, and oxygen counterflow diffusion flames at a=1000 s^{-1}, p=1.01 MPa. The vertical dashed lines signify the location of the stagnation planes.
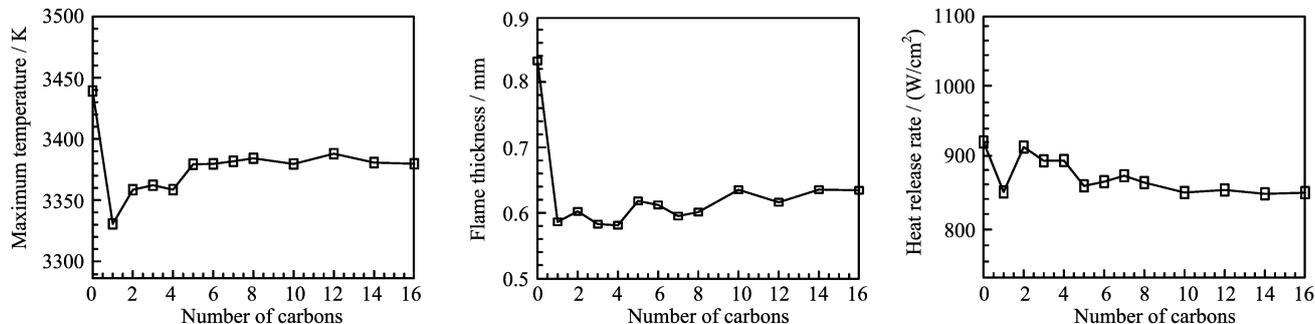
FIG. 3 Effects of number of carbon on maximum temperature, flame thickness, and heat release rate at $a=1000$ s^{-1}, $p=1.01$ MPa.
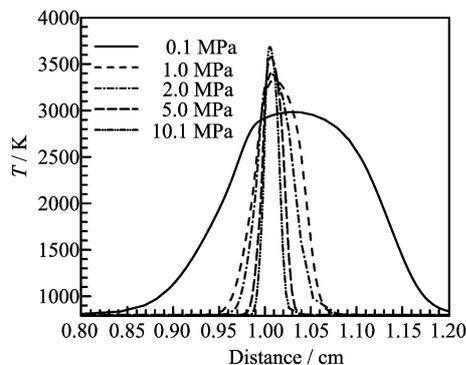

FIG. 4 Temperature profiles of different pressures for CH$_4$/O$_2$ counterflow diffusion, $a=1000$ s^{-1}.
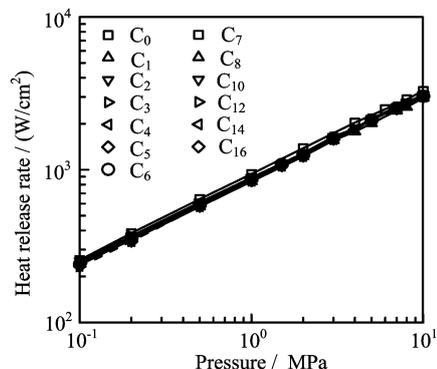
FIG. 6 Heat release rate as a function of pressure for H$_2$, C$_1$−C$_{16}$ n-alkane counterflow diffusion flames, $a=1000$ s^{-1}.
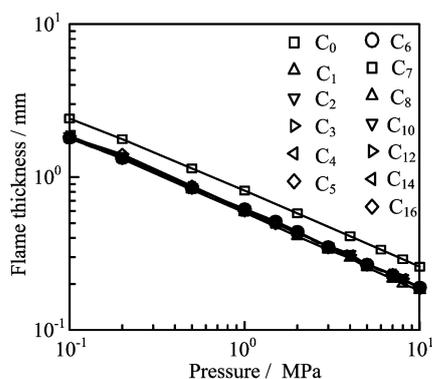
FIG. 5 Flame thickness as a function of pressure for H$_2$, C$_1$−C$_{16}$ n-alkane counterflow diffusion flames, $a=1000$ s^{-1}.
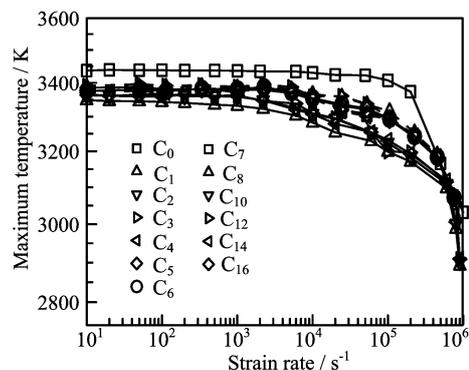
FIG. 7 Effect of strain rate on maximum temperature for H$_2$, C$_1$−C$_{16}$ n-alkane counterflow diffusion flames, $p=1.01$ MPa.

versus strain rate at a typical pressure of 1.01 MPa. At low strain rate, T_{max} remains nearly constant for all of the fuels. At higher strain rate, T_{max} decreases progressively to reach its extinction temperature. H$_2$ always has the highest maximum flame temperature of hydrocarbons at any strain rate point. From C$_1$ to C$_{16}$ the maximum flame temperature increase slightly, but the difference is limited. The effects of strain rate on the flame thickness are shown in Fig.8. The result shows the flame thickness decreases with the strain rate. Ob-

viously, the strain rate has linear dependences of the flame thickness for all the fuels, and hydrocarbons have the same flame thickness and H$_2$ has the thicker flame at any strain rate point.

The reduction in flame thickness with pressure and strain rate had been discovered in some other studies by Law and Ribert [1, 42]. They suggested the use of the pressure-weighted strain rate in correlating their effects. The flame thickness is thus proportional to $1/\sqrt{pa}$. The results of this work also show this rela-
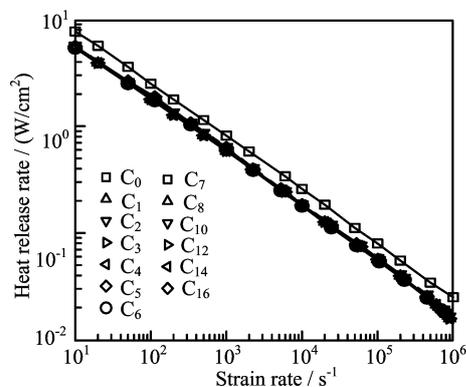
FIG. 8 Flame thickness as a function of strain rate for H_2, C_1-C_{16} n-alkane counterflow diffusion flames, p=1.01 MPa.
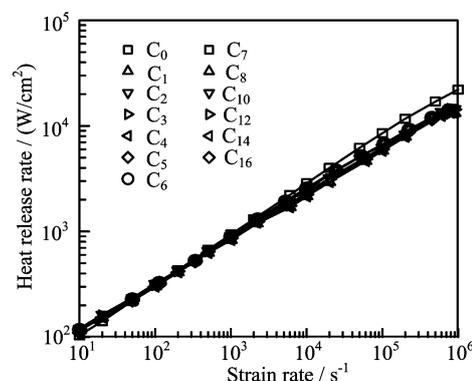
FIG. 10 Heat release rate per unit area as a function of strain rate for H_2, C_1-C_{16} n-alkane counterflow diffusion flames, p=1.01 MPa.
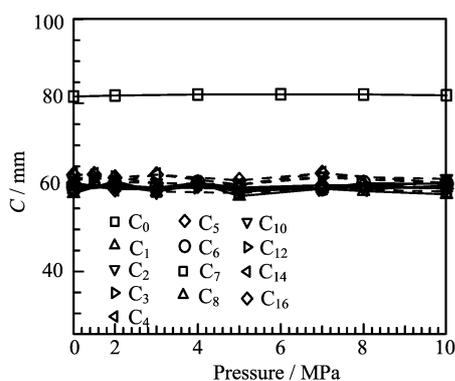

FIG. 9 Counterflow diffusion C for H_2, C_1-C_{16} n-alkane fuels, a=1000 s^{-1}.

tionship. Furthermore, Fig.9 shows the flame thickness parameter $C=\delta_f\sqrt{pa}$, as a function of the pressure ranging 0.10$-$10.1 MPa at strain rate of 1000 s^{-1}. The parameters for the hydrocarbon fuels nearly locate at the same value about 60.

Heat release rate per unit area $\dot{q}_s$ is shown as a function of strain rate in Fig.10 at the typical pressure of 1.01 MPa. For a given pressure, $\dot{q}_s$ increases linearly with the strain rate. It can also be seen that for all the n-alkane hydrocarbons, $\dot{q}_s$ are almost the same at any strain rate point. Combining with the relationship between the heat release rate and pressure obtained above, the results in this work also reveal the functional relationships of $\dot{q}_s$-$\sqrt{pa}$ for all the fuels, and all the n-alkane fuels have a single formula between $\dot{q}_s$ and $\sqrt{pa}$.

The analysis and results above show the flame structure, the flame thickness and the heat release rate are almost the same for all the n-alknae hydrocarbon fuels at any condition. This phenomenon further gives a valuable information that the blend fuels composed with these hydrocarbons will have the same flame properties as a pure n-alkane fuel.

IV. CONCLUSION

A comprehensive analysis of laminar H_2, C_1-C_{16} n-alkane hydrocarbon counterflow diffusion flames has been performed. The corresponding detailed reaction mechanisms from Lawrence Livermore National Laboratory are used. The largest mechanism contains 2115 species and 8157 reversible reactions. The converged solutions of large range of conditions (pressure: 0.1$-$10.1 MPa, strain rate: $10-10^6$ s^{-1}) are obtained. The basic diffusion flame structures have been demonstrated and analyzed, and the effects of pressure, strain rate on the flame behavior and energy-release rate were examined. The major conclusions are summarized: (i) For all the fuels, the locations of maximum flame temperatures are almost the same as those of maximum H_2O mole factions. The major products of combustion of H_2 are H_2O and OH, beside these two species. CO, CO_2, and H_2 become the major products for hydrocarbons. Higher hydrocarbon than C_5, C_2H_2 and C_2H_4 also reach notable concentrations. The mole fractions of carbo$n$-containing products increase for higher hydrocarbons. (ii) For all the fuels, the calculated flame thickness δ_f and heat release rate per unit flame area $\dot{q}_s$ were found to depend on the pressure p and strain rate a through the correlations of δ_f-$\sqrt{pa}$ and $\dot{q}_s$-$\sqrt{pa}$, respectively. (iii) H_2/O_2 counterflow diffusion flame is thicker than the hydrocarbon flames, while the hydrocarbons have the similar temperature and main products distributions and almost have the same flame thickness and heat release rate in any condition, which indicates that the fuels composed with these hydrocarbon fuels will still have these flame properties the same as any pure n-alkane fuel. (iv) The flame thickness parameter $C=\delta_f\sqrt{pa}$, for all the hydrocarbon fuels nearly locate at the same value about 60. Results not only enhance the fundamental understanding of the flame properties under various flow conditions and fluid states, but can also be used as a submodel in the treatment of non-premixed turbulent combustion.

V. ACKNOWLEDGMENTS

[1] G. Ribert, N. Zong, V. Yang, L. Pons, N. Darabiha, and S. Candel, Combust. Flame **154**, 319 (2008)

[2] J. Li, Z. Zhao, A. Kazakov, and F. L. Dryer, Int. J. Chem. Kinet. **36**, 566 (2004).

[3] L. Pons, N. Darabiha, S. Candel, G. Ribert, and V. Yang, Combust. Theory Modell. **13**, 57 (2009).

[4] L. Tosatto, B. L. Mantia, H. Bufferand, P. Duchaine, and A. Gomez, Proc. Combust. Inst. **32**, 1319 (2009).

[5] S. C. Li and F. A. Williams, Proc. Combust. Inst. **28**, 1031 (2000).

[6] R. Seiser, H. Pitch, K. Seshadri, W. J. Pitz, and H. J. Curran, *Proceedings of the Combustion Institute*, Vol.28, Pittsburgh, PA: Combustion Institute, 2029 (2000).

[7] R. B. Dakhlia, V. Giovangigli, and D. E. Rosner, Combust. Theory Modell. **6**, 1 (2002).

[8] H. Xue and S. K. Aggarwal, AIAA J. **11**, 2289 (2002).

[9] X. Zhu and J. P. Gore, AIAA J. **7**, 1491 (2004).

[10] S. Liu, J. C. Hewson, J. H. Chen, and H. Pitsch, Combust. Flame **137**, 320 (2004).

[11] S. Liu, J. C. Hewson, and J. H. Chen, Combust. Flame **145**, 730 (2006).

[12] P. Berta, S. K. Aggarwal, I. K. Puri, S. Granata, T. Faravelli, and E. Ranzi, J. Propul. Power **4**, 797 (2008).

[13] J. M. Card and F. A. Williams, Combust. Flame **91**, 187 (1992).

[14] M. Bolling, H. Pitsch, J. Hewson, and K. Seshadri, Proc. Combust. Inst. **26**, 729 (1996).

[15] S. C. Li, P. A. Libby, and F. A. Williams, *Twenty-Fourth Symposium (International) on Combustion*, Pittsburgh: The Combustion Institute, 1503 (1992).

[16] M. Bui and K. Seshadri, Combust. Sci. Technol. **79**, 293 (1991).

[17] H. K. Chelliah, P. M. Bui, K. Seshadri, and C. K. Law, Proc. Combust. Inst. **24**, 851 (1992).

[18] R. P. Lindstedt and L. Q. Maurice, Combust. Sci. Technol. **107**, 317 (1995).

[19] P. A. Glaude, V. Warth, R. Fournet, F. Batti*n*-Leclerc G. Scacchi, and G. M. Come, Int. J. Chem. Kinet. **30**, 949 (1998).

[20] H. J. Curran, P. Gaffuri, W. J. Pitz, and C. K. Westbrook, Combust. Flame **129**, 253 (2002).

[21] G. Bikas and N. Peters, Combust. Flame **126**, 1456 (2001).

[22] Z. Zhao, J. Li, A. Kazakov, S. P. Zeppieri, and F. L. Dryer, Combust. Sci. Technol. **177**, 89 (2004).

[23] V. P. Zhukov, V. A. Sechenov, and A. Y. Starikovskii, Combust. Flame **153**, 130 (2008).

[24] C. K. Westbrook, W. J. Pitz, O. Herbinet, H. J. Curran, and E. J. Silke, Combust. Flame **156**, 181(2009).

[25] H. S. Shen, J. Steinberg, J. Vanderover, and M. A. Oehlschlaeger, Energy Fuels **23**, 2482 (2009).

[26] K. Kumar, G. Mittal, and C. J. Sung, Combust. Flame **156**, 1278 (2009).

[27] V. P. Zhukov, Combust. Flame **156**, 1674 (2009).

[28] X. You, F. N. Egolfopoulos, and H. Wang, Proc. Combust. Inst. **32**, 403 (2009).

[29] T. Lu, C. K. Law, C. S. Yoo, and J. H. Chen, Combust. Flame **156**, 1542 (2009).

[30] J. M. Simmie, Prog. Energy Combust. Sci. **29**, 599 (2003).

[31] E. Ranzi, P. Gaffuri, T. Faravelli, and P. Dagaut, Combust. Flame **103**, 91 (1995).

[32] H. J. Curran, P. Gaffuri, W. J. Pitz, and C. K. Westbrook, Combust. Flame **114**, 149 (1998).

[33] H. S. Shen, J. Steinberg, J. Vanderover, and M. A. Oehlschlaeger, Energy Fuels **23**, 2482 (2009).

[34] K. Kumar, G. Mittal, and C. Sung, Combust. Flame **156**, 1278 (2009).

[35] M. O. Conaire, H. J. Curran, J. M. Simmie, W. J. Pitz, and C. K. Westbrook, Int. J. Chem. Kinet. **36**, 603 (2004).

[36] N. M. Marinov, W. J. Pitz, C. K. Westbrook, A. M. Vincitore, M. J. Castaldi, and S. M. Senkan, Combust. Flame **114**, 192 (1998).

[37] N. Peters, *Turbulent Combustion*, Cambridge: Cambridge University Press, (2000).

[38] https://www-pls.llnl.gov/?url=science_and_technology-chemistry-combustion, Cited 13 October (2010).

[39] R. J. Kee, F. M. Rupley, J. A. Miller, M. E. Coltrin, J. F. Grcar, E. Meeks, H. K. Moffat, A. E. Lutz, G. Dixo*n*-Lewis, M. D. Smooke, J. Warnatz, G. H. Evans, R. S. Larson, R. E. Mitchell, L. R. Petzold, W. C. Reynolds, M. Caracotsios, W. E. Stewart, P. Glarborg, C. Wang, C. L. McLellan, O. Adigun, W. G. Houf, C. P. Chou, S. F. Miller, P. Ho, P. D. Young, D. J. Young, D. W. Hodgson, M. V. Petrova, and K. V. Puduppakkam, *CHEMKIN-PRO Release*, San Diego, CA: Reaction Design, Inc., 15082 (2008).

[40] A. E. Lutz, R. J. Kee, J. F. Grcar, and F. M. Rupley, *Sandia National Lab.*, Sandia Rept. SAND96-8243, May (1997).

[41] K. Seshadri and F. A. Williams, Int. J. Heat Mass Trans. **21**, 251 (1978).

[42] C. K. Law, Combust. Sci. Technol. **178**, 335 (2006).